Biomimicry-inspired Fish Scale-like Ni$_3$N/FeNi$_3$N/NF Superhydrophilic/Superaerophobic Nanoarrays Displaying High Electrocatalytic Performance

Yucheng Dong[a], yutai Wu[a], Xuyun Wang[a,*], Hui Wang[a], Jianwei Ren[b,*], Peng Wang[c], Lei Pan[c], Guoqiang Wang[c], Rongfang Wang[a*]

[a] *State Key Laboratory Base for Eco-Chemical Engineering, College of Chemical Engineering, Qingdao University of Science and Technology, Qingdao, 266042, China.*
[b] *Department of Mechanical Engineering Science, University of Johannesburg, Cnr Kingsway and University Roads, Auckland Park, 2092, Johannesburg, South Africa.*
[c] *Shandong Hydrogen Energy CO., Ltd, Weifang, 261000, China.*

Experimental

1. Preparation of Ni_3N/NF sample

Similarly, the treated nickel foam (NF) was immersed in 20 mL of dilute HCl (3.6×10^{-3} M HCl) solution, and the mixture was transferred to a 100 mL reaction autoclave. The autoclave was then heated up to 100 °C and kept at that temperature for 20 h. After the reaction, the sample was collected, washed with ultrapure water and dried under vacuum at 60 °C. The obtained sample was marked as $Ni(OH)_2/NF$. Sequentially, the dried $Ni(OH)_2/NF$ sample was placed on the top of the porcelain boat in a tube furnace. After the alternative purging by N_2 for 15 min and NH_3 for 15 min with gas velocity of 20 mL min^{-1}, the tube furnace was then heated to 400 °C at 10 °C min^{-1} and maintained at that temperature for 60 min to yield the Ni_3N/NF sample.

2. Preparation of NF-N sample

The treated nickel foam was placed into a porcelain boat in the tube furnace. After the alternative purging by N_2 for 15 min and NH_3 for 15 min with gas velocity of 20 mL min^{-1}, the tube furnace was then heated to 400 °C at 10 °C min^{-1} and maintained at that temperature for 60 min. The resultant product was labeled as NF-N sample.

3.Physical characterizations

The morphology of newly prepared materials was studied by field-emission scanning electron microscopy (SEM) on a Carl Zeiss Ultra Plus system. Using the CAST 3.0 system, using a 25-gauge pinhole, the contact angle of the bubble under the electrolyte was measured by the trapped bubble method, and the Axisymmetric Drop Shape Analysis young laplace equation was used for fitting, and the wetting of the electrolyte was measured by the pendant drop method at 0.8 cm.The X-ray diffraction (XRD) was done on Shimadzu XD-3A Instrument, which was fitted with filtered Cu-Kα radiation ($\lambda = 0.15418$ nm) and operated at 30 mA and 40 kV. The 2θ scan rate for XRD analysis was set at 5 ° min^{-1}. JEOL (JEM-2000 FX) microscope operated at 200 kV was used for transmission electron microscopy (TEM), high angle annular dark field scanning transmission electron microscopy (STEM) images and selected area electron diffraction (SAED) analysis. X-ray photoelectron spectra (XPS) were carried out on VG Escalab210 Spectrometer with Mg 300 W X-ray source. Brunauer-Emmett-Teller (BET) was used to measure the specific surface area of all the prepared samples, and

density functional theory (DFT) method was used to calculate the pore size distribution of materials. The ultraviolet photoelectron spectra (UPS) of samples were recorded using HeI irradiation with hv = 21.21 eV on a ThermoFisher ESCALAB 250Xi spectrometer.

4.Electrochemical Characterization

All electrochemical measurements were performed with Hg/HgO as the reference electrode and a graphite rod as the counter electrode. The measured potential was converted to a reversible hydrogen electrode (RHE) using the equation $E_{RHE}=E_{Hg/HgO}+0.059pH+0.098$ V. Linear sweep voltammetry (LSV) tests were performed at a scan rate of 5 mV s^{-1} and all polarization curves were IR compensated (100%). Chemical Impedance Spectroscopy (EIS) was tested in the frequency range of 0.01 Hz – 100 kHz. The electrochemical double layer capacitance (C_{dl}) of the samples was determined by cyclic voltammetry (CV) in the Faradaic potential range. Current-time responses were obtained by chronopotentiometry (CP) testing at a current density of 50 mA cm^{-2} for 100 h.
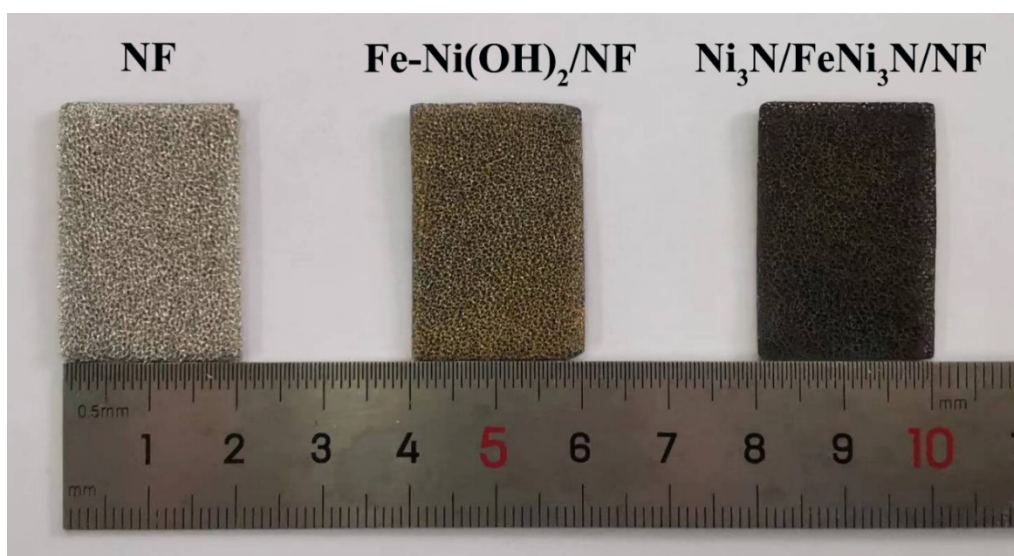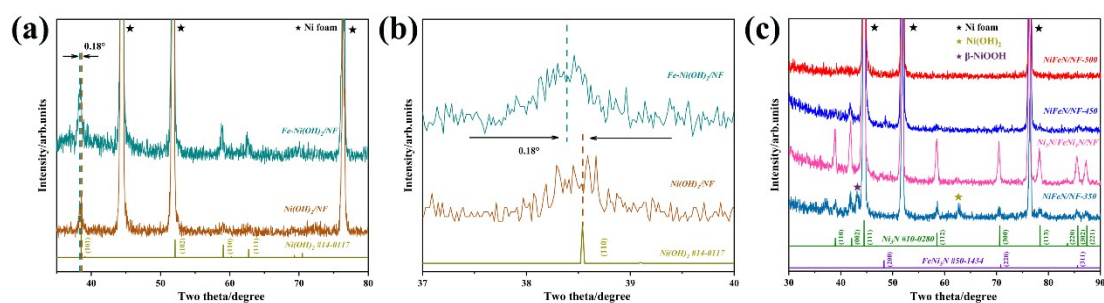

Fig. S1. Morphological photos of the NF, Fe-Ni(OH)$_2$/NF and Ni$_3$N/FeNi$_3$N/NF samples
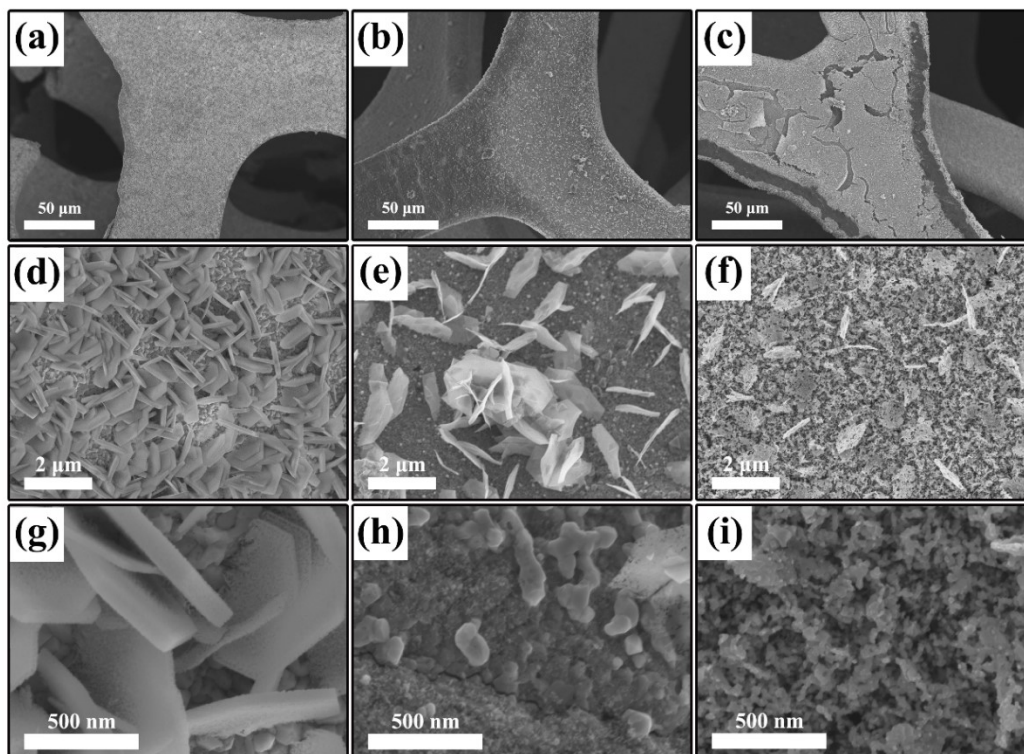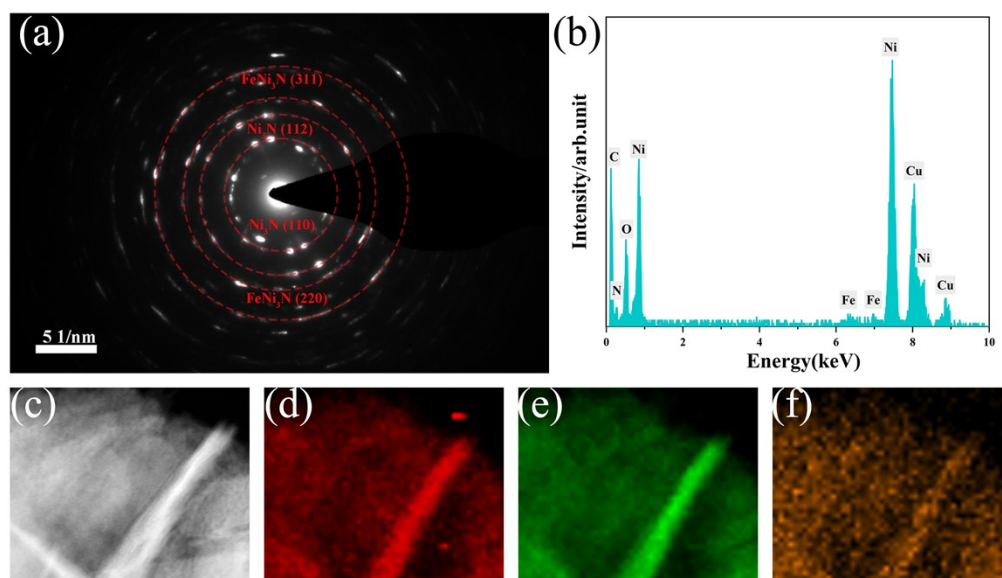
**Fig. S2**. SEM images of samples: (a, d, g) NiFeN/NF-350, (b, e, h) NiFeN/NF-450 and (c, f, i) NiFeN/NF-500.
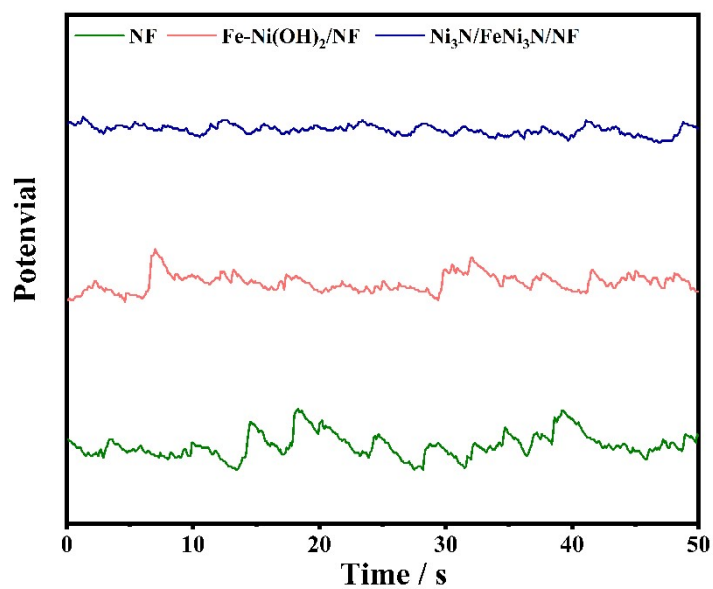
**Fig. S3.** CP measurements of NF, Fe-Ni(OH)$_2$/NF, Ni$_3$N/FeNi$_3$N/NF samples at current density of 800 mA cm^{-2}.

Fig. S4. XRD patterns of: (a) Fe-Ni(OH)$_2$/NF and Ni(OH)$_2$/NF samples; (b) Fe-Ni(OH)$_2$/NF and Ni(OH)$_2$/NF samples (partially enlarged); (c) NiFeN/NF-350, Ni$_3$N/FeNi$_3$N/NF, NiFeN/NF-450, and NiFeN/NF-500 samples.


Fig. S5. (a) SAED patterns; (b) EDX spectrum of the Ni$_3$N/FeNi$_3$N/NF sample. (c) STEM and electron energy loss spectroscopy (EELS) elemental mappings of (d) N, (e) Ni and (f) Fe.
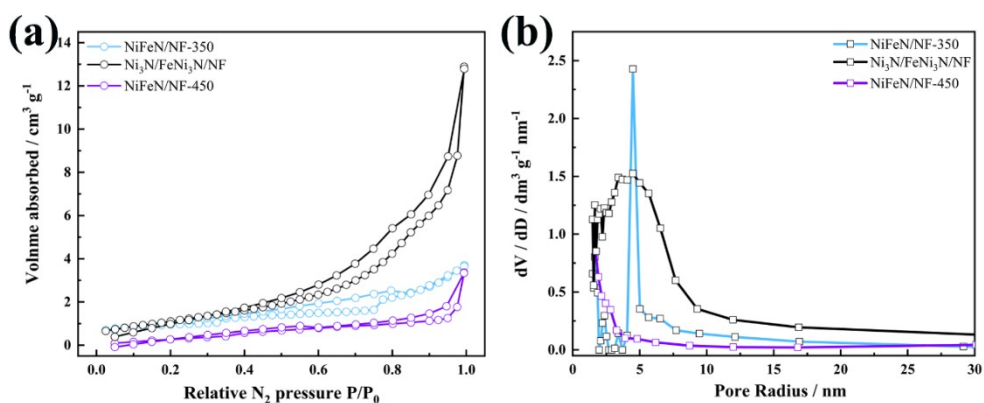
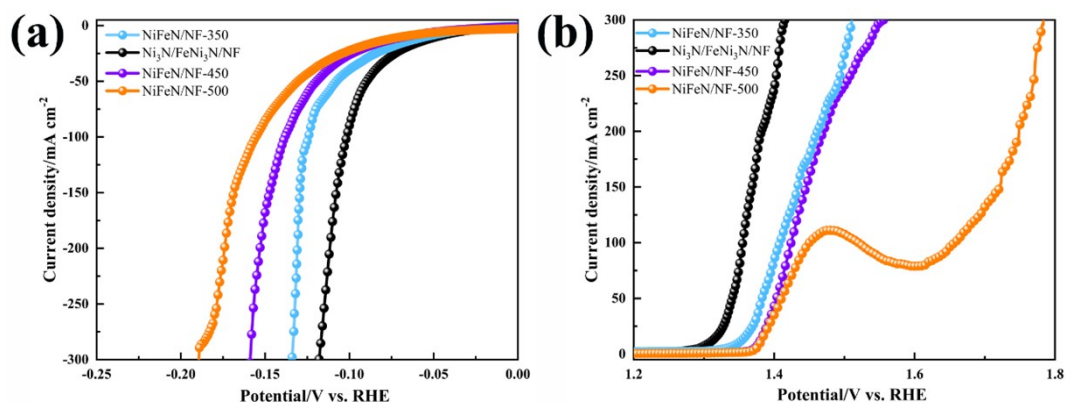**Fig. S6**. (a) N_2 adsorption-desorption isotherms and (b) Pore-size-distribution curves of three samples.
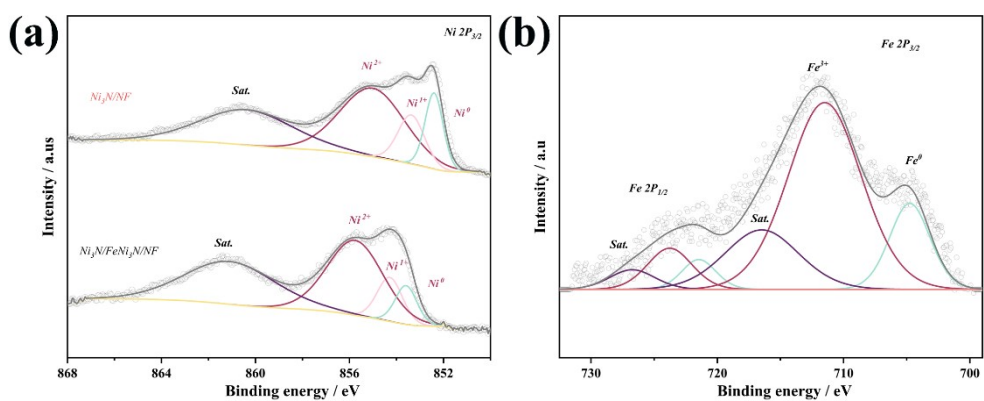
Fig. S7. The deconvoluted high-resolution XPS spectra of: (a) Ni $2p_{3/2}$ of the Ni_3N/NF and $Ni_3N/FeNi_3N/NF$ samples. (b) Fe 2p of the $Ni_3N/FeNi_3N/NF$ sample.
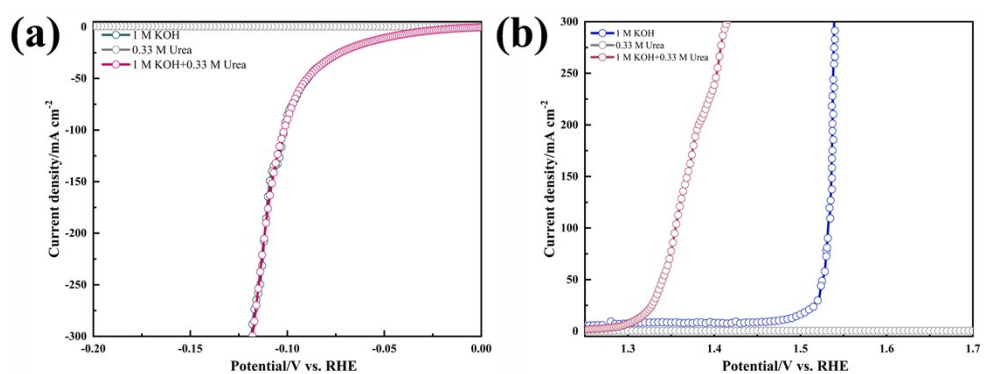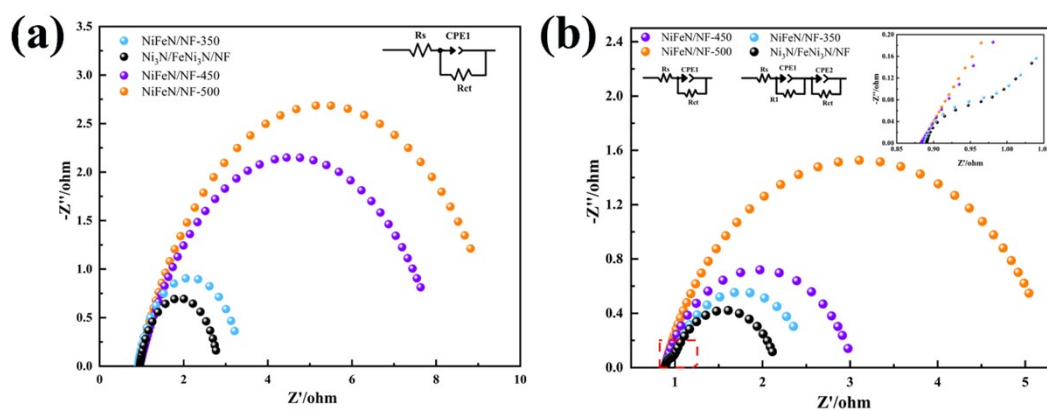

Fig. S8. Comparing (a) HER and (b) OER curves of $Ni_3N/FeNi_3N/NF$ sample in 1M KOH with and without 0.33M urea at a scan speed of 5 mV s^{-1}.
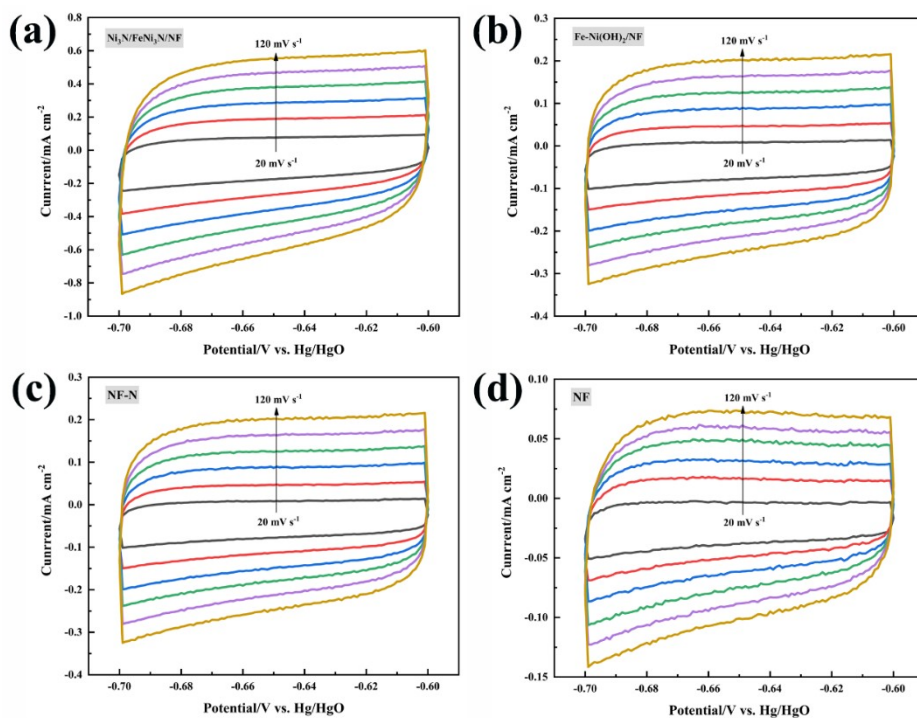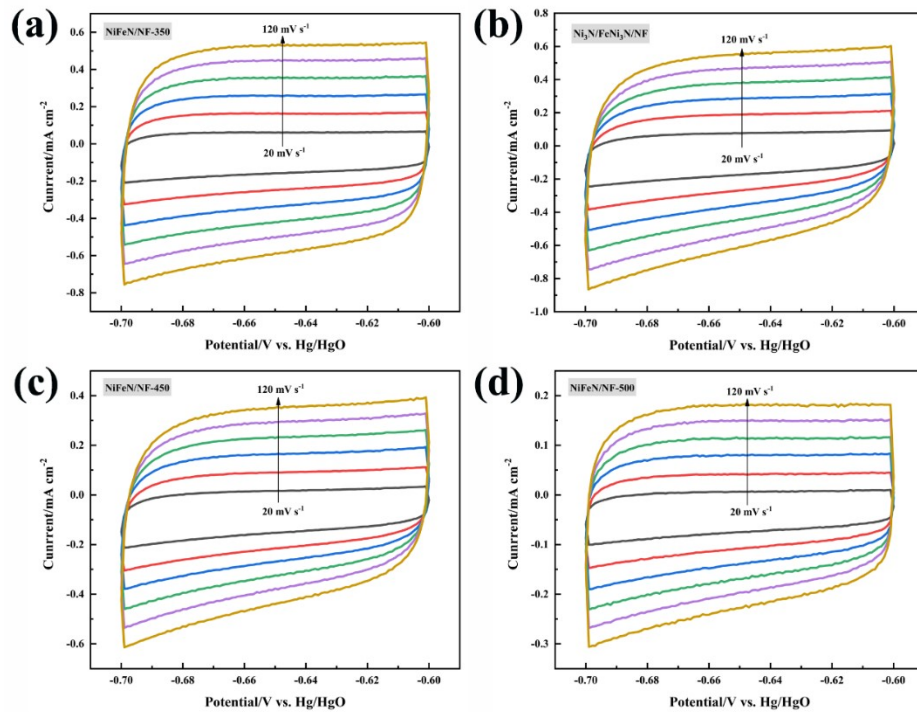
Fig. S9. (a) HER and (b) UOR LSV curves of the NiFeN/NF-350, $Ni_3N/FeNi_3N/NF$, NiFeN/NF-450 and NiFeN/NF-500 samples synthesized at different nitridation temperatures.

Fig. S10. Nyquist plots of (a) HER and (b) UOR of the NiFeN/NF-350, $Ni_3N/FeNi_3N/NF$, NiFeN/NF-450 and NiFeN/NF-500 samples synthesized at different nitridation temperatures.

Fig. S11. The CV curves of (a) Ni$_3$N/FeNi$_3$N/NF, (b) Fe-Ni(OH)$_2$/NF, (c) NF-N and (d) NF samples.

Fig. S12. The CV curves of (a) NiFeN/NF-350, (b) Ni$_3$N/FeNi$_3$N/NF, (c) NiFeN/NF-450 and (d) NiFeN/NF-500 samples.
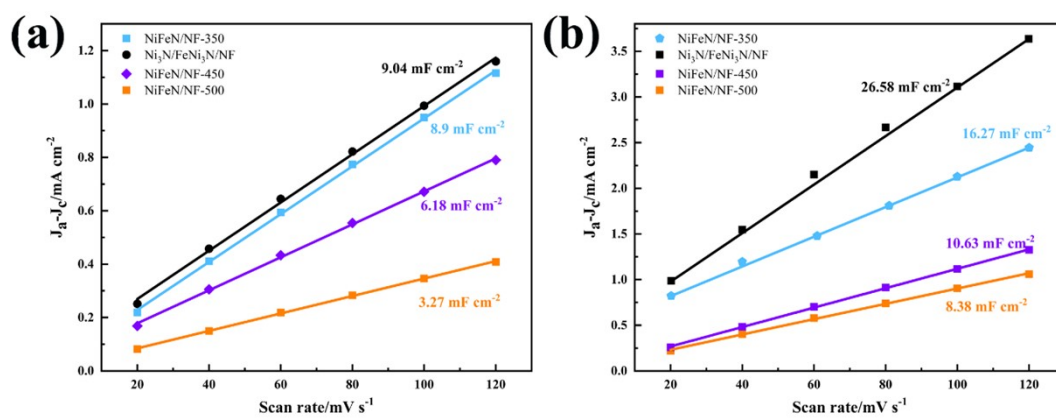
Fig. S13. Linear fitting of: (a) HER △j vs. scan rates at 0.316 V vs. RHE, and (b) UOR

△j vs. scan rates at 0.716 V vs. RHE.
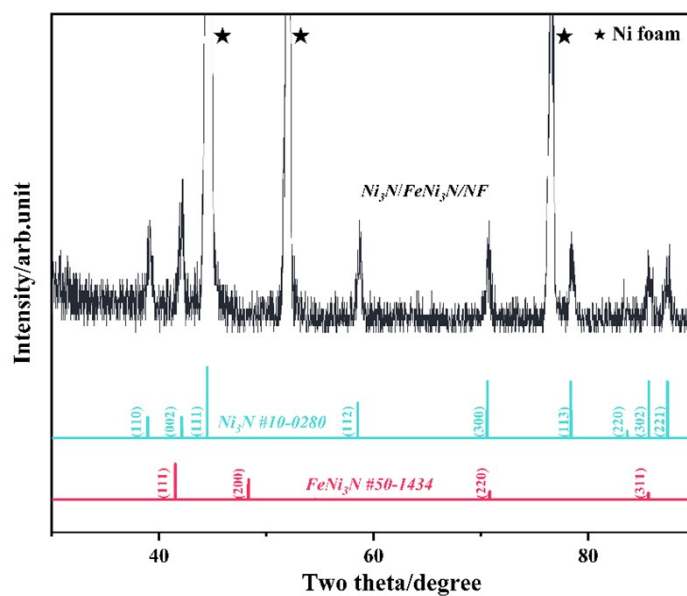
Fig. S14. The XRD pattern of the $Ni_3N/FeNi_3N/NF$ sample after stability test.
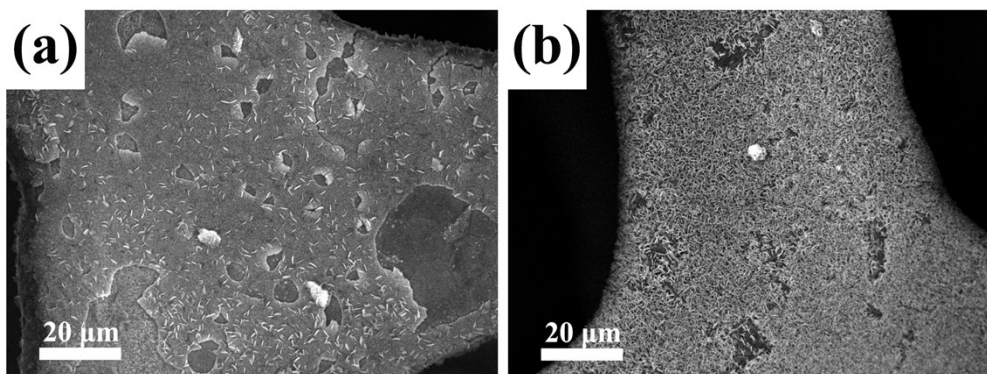
Fig. S15. SEM images of samples: (a) Fe-Ni(OH)$_2$/NF and (b) Ni$_3$N/FeNi$_3$N/NF after stability test.
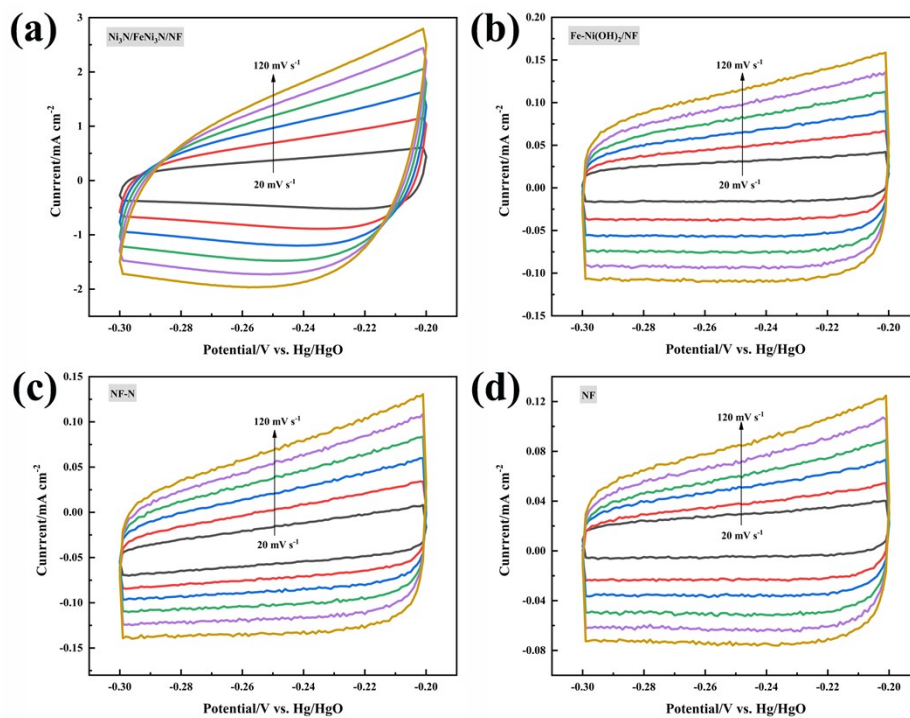
Fig. S16. CV curves of the (a) Ni$_3$N/FeNi$_3$N/NF, (b) Fe-Ni(OH)$_2$/NF, (c) NF-N and (d) NF samples.
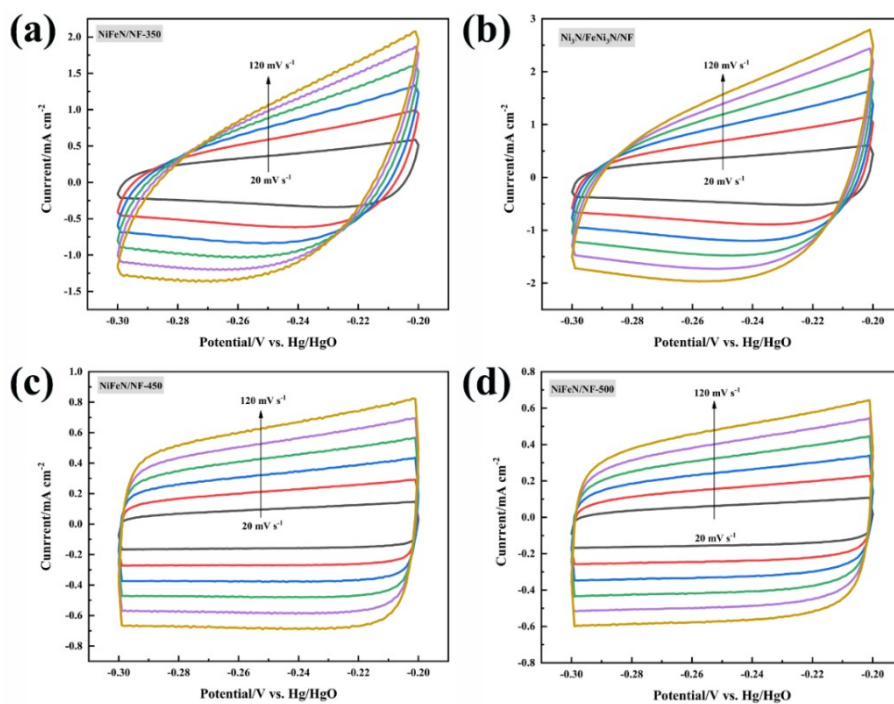
Fig. S17. CV curves of the (a) NiFeN/NF-350, (b) Ni₃N/FeNi₃N/NF, (c) NiFeN/NF-450 and (d) NiFeN/NF-500 samples.
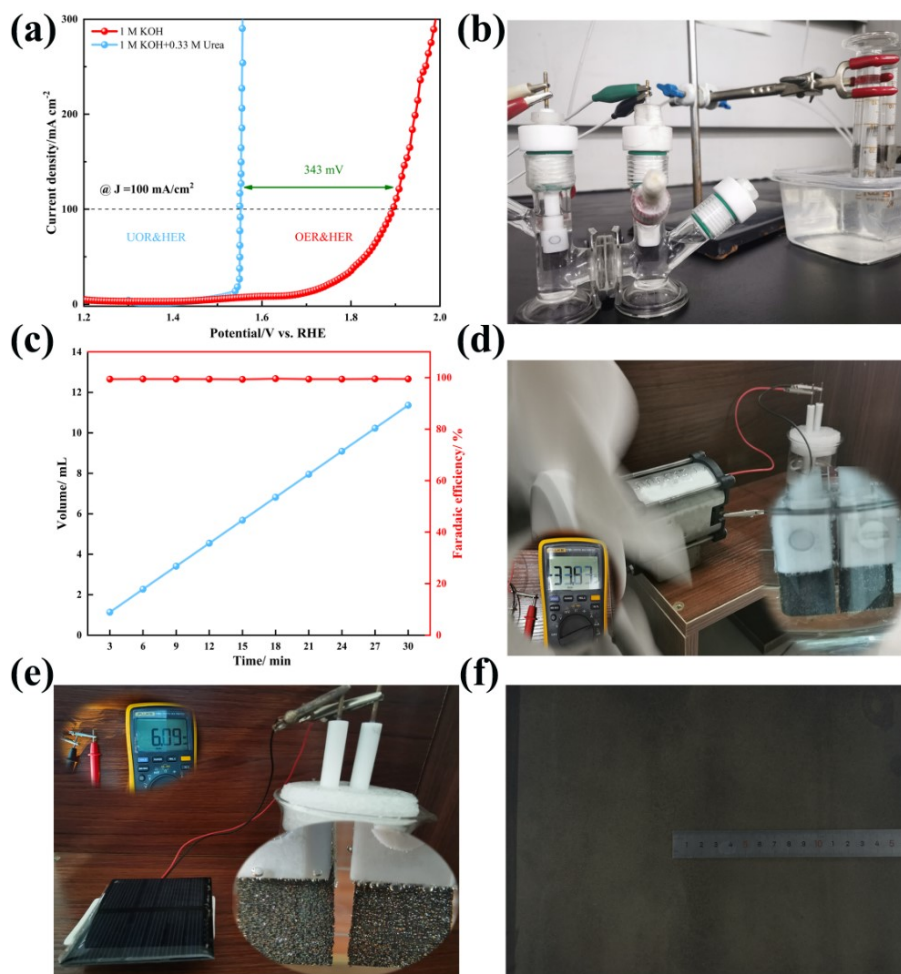
Fig. S18. (a) $Ni_3N/FeNi_3N/NF$ sample as bi-electrode. (b) Two-electrode device of UOR. (c) Variation of the volume of H_2 produced over time and the corresponding Faradaic efficiency. (d, e) Using solar and wind energy as renewable resources to drive electrolytic urea systems, respectively. (f) A scaled-up experiment with a size of 25 cm × 25 cm.

Table S1 The comparison of basic HER activities of electrocatalysts in different systems.

HER catalysts	Morphology	₥, HER (mV)	Ref.
$Ni_3N/FeNi_3N/NF$	Nanosheets	48@10, 102@100	This work
$Ni_{0.67}Co_{0.33}/Ni_3S_2@NF$	Nanosheets	87@10, 203 mV@100	[1]
$MnCo-P_3/NF$	Nest-like porous	47@10, 112@100	[2]
$NiCoP/NiCoS_x/NF$	Nanosheets	68@10, 144@100	[3]
$NiS-Ni_2P/Ni/NF$	Coil-like	53@10, 139@100	[4]
$NiMoO_4-200/NF$	Urchin-like nanorod	68@10, 242@100	[5]
$Co/CoMoN/NF$	Nanosheets	61@10, 173@100	[6]
F-FeCoNi-Ov LDH/NF	Nanosheets	109@10, 207@100	[7]
TiO_2-CoP/NF	Nanoneedle-like	61@10, 127@100	[8]
NiMoCu-NF	Nanosheets	52@10, 200@100	[9]
NiMoN/NiN	Nano stave	49@10, 136@100	[10]
Ni–Ce–Pr–Ho/NF	Nami Island	78@10	[11]
50MCNP@NF	Nanosheets	93@10, 170@100	[12]

Table S2. Activity comparison of different electrocatalysts in 1M KOH+0.33M Urea.

UOR catalysts	Morphology	Ŋ, UOR (V)	Ref.
$Ni_3N/FeNi_3N/NF$	Nanosheets	1.30@10, 1.35@100	This work
NiFe-PBA/NF	Dart shape	1.34@10, 1.37@100	[13]
$NiO/Ni_2P/NF$-40	Nanosheets	1.34@10, 1.38@100	[14]
NiFe NSs/NF	Nanosheets	1.33@10, 1.37@100	[15]
NiCu-P/NF and NiCu-Pi/NF	Nanosheets	1.41@10, 1.56@100	[16]
CoFe-250	Nanoneedles	1.30@10, 1.37@100	[17]
Cu/Fe-MOFs	Nano-particles	1.37@10, 1.43@100	[18]
NiMoCu-NF	Dendrite arrays	1.35@10, 1.4@100	[9]
FeNi-MOF NSs	Nanosheets	1.36@10, 1.39@100	[19]
FeCo-LDH	Nanosheets	1.33@10, 1.38@100	[20]
Cu-doped Ni_3S_2/NF	Nanosheets	1.30@10, 1.42@100	[21]
P-NTS-0.5	flower-like	1.36@10, 1.55@100	[22]

References

1. Z. Wu, Y. Feng, Z. Qin, X. Han, X. Zheng, Y. Deng and W. Hu, *Small*, **n/a**, 2106904.

2. D. Guo, D. Duan, J. Gao, X. Zhou, S. Liu and Y. Wang, *Int. J. Hydrog. Energy*, 2022, **47**, 6620-6630.

3. W. Han, F. Zhang, L. Qiu, Y. Qian, S. Hao, P. Li, Y. He and X. Zhang, *Nanoscale*, 2022, DOI: 10.1039/D2NR04657A.

4. M. Liu, Z. Sun, C. Zhang, S. Li, C. He, Y. Liu and Z. Zhao, *J. Mater. Chem. A*, 2022, **10**, 13410-13417.

5. C. Chen, S. He, K. Dastafkan, Z. Zou, Q. Wang and C. Zhao, *Chinese J. Catal.*, 2022, **43**, 1267-1276.

6. H. Ma, Z. Chen, Z. Wang, C. V. Singh and Q. Jiang, *Adv. Sci.*, 2022, **9**, 2105313.

7. Z. Zhai, W. Yan and J. Zhang, *Nanoscale*, 2022, **14**, 4156-4169.

8. M. Deng, H. Yang, L. Peng, L. Zhang, L. Tan, G. He, M. Shao, L. Li and Z. Wei, *J. Energy Chem.*, 2022, **74**, 111-120.

9. R. Li, Y. Yuan, H. Gui, Y. Liu, H. Li, Y. Li, S. Wen, A. Liu, J. Zhang, P. Yang and M. An, *Nanoscale*, 2022, **14**, 14297-14304.

10. B. Wang, L. Guo, J. Zhang, Y. Qiao, M. He, Q. Jiang, Y. Zhao, X. Shi and F. Zhang, *Small*, 2022, **18**, 2201927.

11. W. Liu, W. Tan, H. He, Y. Peng, Y. Chen and Y. Yang, *Energy*, 2022, **250**, 123831.

12. Y. Zhang, H. Liu, R. Ge, J. Yang, S. Li, Y. Liu, L. Feng, Y. Li, M. Zhu and W. Li, *Sustain. Mater. Technol.*, 2022, **33**, e00461.

13. X. Jia, H. Kang, X. Yang, Y. Li, K. Cui, X. Wu, W. Qin and G. Wu, *Appl. Catal. B*, 2022, **312**, 121389.

14. X. Xu, S. Ji, H. Wang, X. Wang, V. Linkov and R. Wang, *J. Colloid Interface Sci.*, 2022, **615**, 163-172.

15. Y. Diao, Y. Liu, G. Hu, Y. Zhao, Y. Qian, H. Wang, Y. Shi and Z. Li, *Biosens. Bioelectron.*, 2022, **211**, 114380.

16. X. Xu, S. Ji, H. Wang, X. Wang, V. Linkov, P. Wang, L. Pan, G. Wang and R. Wang, *Nanoscale*, 2022, DOI: 10.1039/D2NR04409A.

17. Q. Zhang, M. Sun, J. Zhu, S. Yang, L. Chen, X. Yang, P. Wang, K. Li, F. Xue, Y. Lu, J. Zhang and P. Zhao, *Chem. Eng. J.*, 2022, **432**, 134275.

18. S. A. Patil, N. K. Shrestha, A. I. Inamdar, C. Bathula, J. Jung, S. Hussain, G. Nazir, M. Kaseem, H. Im and H. Kim, *Nanomaterials*, 2022, **12**, 1916.

19. X. Zhang, X. Fang, K. Zhu, W. Yuan, T. Jiang, H. Xue and J. Tian, *J. Power Sources*, 2022, **520**, 230882.

20. Y. Gong, H. Zhao, D. Ye, H. Duan, Y. Tang, T. He, L. A. Shah and J. Zhang, *Appl. Catal. A Gen.*, 2022, **643**, 118745.

21. M. Wei, D. Zhang, J. Deng, X. Xiao, L. Wang, X. Wang, M. Song, S. Wang, X. Zheng and X. Liu, *Ind. Eng. Chem. Res.*, 2022, **61**, 7777-7786.

22. Z. Ji, J. Liu, Y. Deng, S. Zhang, Z. Zhang, P. Du, Y. Zhao and X. Lu, *J. Mater. Chem. A*, 2020, **8**, 14680-14689.